Japanese Journal of Applied Physics
Vol. 43, No. 11A, 2004, pp. 7546–7551

Ultrafast Electron Dynamics in GaAs and InP Studied by Time-Resolved Terahertz Emission Spectroscopy

Toshiaki HATTORI*, Satoshi ARAI and Keiji TUKAMOTO

Institute of Applied Physics, University of Tsukuba, Tsukuba 305-8573, Japan

(Received June 14, 2004; accepted August 6, 2004; published November 10, 2004)

We studied the ultrafast dynamics of electrons generated by tunable femtosecond optical pulses having positive and negative excess energies in GaAs and InP by observing the temporal waveform of THz radiation emitted from biased photoconductive antennas. Sub-picosecond intraband relaxation was observed when the excess energy was positive. When excited by optical pulses having negative excess energies, it was observed that the THz waveform had a picosecond decay, which was attributed to the transition from the Urbach state to the free carrier state of electrons on the picosecond time scale. This dynamical behavior was found to be very sensitive to the applied electric field in the range of several kV/cm. The largest THz signal was obtained by pumping the emitter at the band-gap energy. [DOI: 10.1143/JJAP.43.7546]

KEYWORDS: terahertz radiation, GaAs, Urbach tail, electron dynamics

1. Introduction

The ultrafast dynamics of carriers in semiconductors are of great importance for understanding fundamental physics and for applications of semiconductors in high-speed electronic devices, and have been studied extensively using various ultrafast nonlinear spectroscopic techniques, such as pump–probe, four-wave mixing, and transient Raman measurements,[1–4] and also using simulations.[5,6] Recently, techniques for the generation and detection of THz electromagnetic radiation using femtosecond optical pulses have been developed,[7–16] and are widely used in spectroscopy and imaging. In these applications, biased or unbiased semiconductors are most often used as emitter materials. In these emitter materials, the transient current generated by ultrashort optical pulses serves as the source of THz radiation. This implies that the magnitude and the temporal waveform of the emitted THz pulses carry substantial information concerning the ultrafast dynamics of the coherent motions of the photogenerated carriers in the emitter materials. Thus far, several studies on ultrafast electron dynamics using THz emission spectroscopy have been reported.[17–22] In these studies, a high bias field (typically several tens of kV/cm) was applied to the semiconductor materials with a very narrow electrode spacing (0.5–4 μm), and the interesting characteristics of carrier dynamics under a high electric field, such as overshoot effects, were observed.

In the present study, we adopted a different structure, a large-aperture photoconductive antenna, as the THz emitter, and observed the ultrafast dynamics of photogenerated electrons in GaAs and InP under a moderate electric field. Large-aperture photoconductive antennas have been used in order to generate an intense THz field[11–16,23–26] for applications such as imaging, Rydberg atom manipulation, and liquid-phase molecular dynamics study. A large-aperture antenna is, however, also used to the study of carrier dynamics in the antenna materials using time-resolved THz emission spectroscopy for the following reasons. First, by focusing the THz radiation emitted from a wide area on a large-aperture emitter surface, a large signal can be obtained under a moderate excitation density, typically $10^{15}\,\mathrm{cm}^{-3}$, and a moderate bias field below 10 kV/cm. Thus, the intrinsic dynamics of carriers, without the influence of carrier-carrier scattering or high-field effects, can be studied. Secondly, the THz waveforms obtained from the large-aperture emitter suffer negligibly from saturation and space-charge screening,[27–29] which often makes the study of the intrinsic dynamics of carriers using small-aperture emitters difficult. Thirdly, the THz radiation emitted from the large-aperture emitter maintains a smooth wave front, which ensures a simple relation between the THz temporal waveform, $E_{\mathrm{THz}}(t)$, and the time dependence of the current density in the emitter material, $J(t)$, as[10,12,13)]

$$E_{\mathrm{THz}}(t) = -\frac{A^2}{2cf}\frac{\eta_0}{1+\sqrt{\varepsilon}}\frac{d}{dt}J(t) \tag{1}$$

to a reasonable approximation. Here, A is the pump beam radius, c is the speed of light, f is the focal length, $\eta_0 = 377\,\Omega$ is the impedance of vacuum, and ε is the dielectric constant of the emitter medium. Thus, the measured waveforms can be directly related to the carrier dynamics in the emitter material.

In this study, we studied the electron dynamics in GaAs and InP by observing the THz waveforms emitted from biased large-aperture photoconductive antennas fabricated using these materials. The emitter materials were excited using 150 fs light pulses to create carriers. By tuning the central photon energy, we observed markedly different behaviors depending on whether the excitation photon energy lay above or below the band-gap energy, i.e., whether the excess energy was positive or negative. Here and throughout this paper, we define the excess energy as the energy difference obtained by subtracting the band-gap energy of the material from the central photon energy of the excitation light spectrum.

The intraband relaxation dynamics of photogenerated carriers with a positive excess energy have been extensively studied using a variety of techniques,[1–4] although many of these studies are concerned with electron dynamics at relatively high excitation densities. Intraband relaxation on the sub-picosecond time scale has been observed from these measurements.

Little is known yet, on the other hand, about the electron dynamics with a *negative* excess energy. Almost all semiconductor materials are known to have a low-energy tail

*E-mail address: hattori@bk.tsukuba.ac.jp

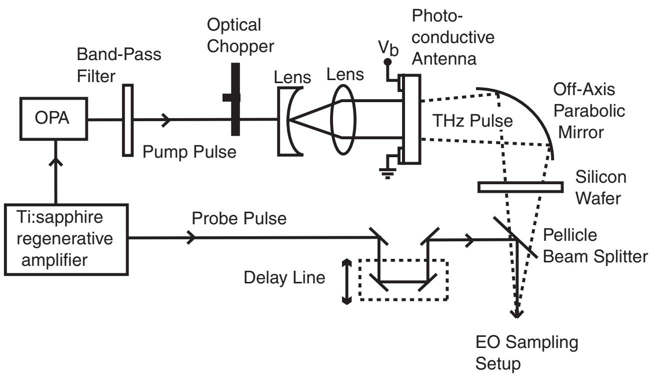

Fig. 1. Schematic of experimental setup for THz waveform measurement. OPA: optical parametric amplifier.

below their fundamental absorption edge, which follows Urbach's rule of[30–35)]

$$\alpha(\omega) = \alpha_0 \exp[(\hbar\omega - E_g)/E_0]. \tag{2}$$

Here, α is the absorption coefficient, ω is the photon angular frequency, E_g is the band-gap energy, and E_0 is the characteristic energy that determines the steepness of the tail. The theoretical explanations of this empirical rule have been given in terms of exciton scattering by acoustic[31,32)] and optical[33–35)] phonons or crystal randomness.[35)] Although these theoretical studies have successfully derived the exponential shape of the absorption spectrum, little is understood on what happens after excitons are created by photons having energies in the region of the Urbach tail. Studies on the absorption edge of GaAs and InP have shown that the Urbach tail of these crystals should be attributed to LO phonon scattering and/or crystal randomness.[33,35,37–40)]

2. Experiments

A schematic of the experimental setup is shown in Fig. 1. A GaAs or InP large-aperture photoconductive antenna[12,13)] with a 3 cm gap between the electrodes was pumped at a repetition rate of 1 kHz using 150 fs tunable optical pulses obtained from an optical parametric amplifier (OPA). The OPA was pumped using the major portion of the regeneratively amplified output of a femtosecond mode-locked Ti:sapphire laser. The residual portion of the regenerative amplifier output was used as the probe pulse of the electrooptic (EO) sampling measurements. The OPA output was expanded spatially by a factor of 4.25 using a combination of concave and convex lenses in order to illuminate a large area of the surface of the antenna materials. The temporal waveform of the electric field of the emitted THz radiation was measured using a standard setup[41)] of the EO sampling method. The thickness of the ZnTe crystal used for the EO sampling was 1 mm. For the calculation of the THz electric field, the following EO constant and ZnTe refractive index were used: $r_{41} = 4.0$ pm/V and $n_0 = 2.85$.[12)]

The photon energy of the OPA output was tuned across the band-gap energy of each material; 1.428 eV for GaAs and 1.351 eV for InP, and the spectral width was narrowed using an interferometric band-pass filter having a bandwidth of 10 nm. The characteristics of the OPA output could not be maintained constant when varying the output wavelength since the optimization of OPA performance by realignment was required at each wavelength. Therefore, the OPA output at each wavelength was characterized by measuring the pulse energy, duration, spectrum, and beam diameter. The pump pulse width measured using second-harmonic autocorrelation was about 150 fs through the tuned wavelength range. The pump pulse energy used in the present study was 1.5–3.0 μJ, which is much lower than the saturation level.[12)] Since the amplitude of the emitted THz field is proportional to the pump photon number at each pump wavelength, all the data presented in this paper are those normalized for a fixed pump photon number which corresponds to that of a pump energy of 3.0 μJ at 1.55 eV. The pump spot size also depended slightly on the wavelength. Knife-edge measurements showed that the intensity distribution of the pump beam was almost Gaussian, and the spot diameter for the $1/e^2$ peak value was 8.0–12.1 mm, depending on the wavelength. Equation (1) shows, however, that the amplitude of the THz field observed at the focus does not depend on the pump spot size when the pump energy is maintained constant. Therefore, we did not correct the data for the wavelength dependence of pump spot size. The photogenerated electron density was estimated to range from 10^{15} to 10^{17} cm^{-3}, depending on the absorption coefficient at the pump wavelength.

The pulse width and the wavelength of the probe pulse were 130 fs and 800 nm, respectively. A Si wafer was placed in the path of the THz radiation in order to block laser light and allow only THz waves to pass. This is necessary for measurements at negative excess energies, where a small portion of the pump light is transmitted through the antenna materials. The pump pulse train was chopped at 500 Hz and the EO sampling signal was lock-in detected at this frequency.

The antennas were fabricated using a 350-μm-thick 2-inch semi-insulating GaAs or InP wafer. The GaAs wafer was grown by the horizontal Bridgman method and doped with CrO. The InP wafer was grown by the liquid-encapsulated Czochralski method and doped with Fe. In both samples, the dopant density was estimated to range from 10^{16} to 10^{17} cm^{-3}. A pulsed bias electric voltage was applied to the wafer through the electrodes. The voltage pulse width was 1 μs, and the amplitude was in the range of 4–28 kV.

3. Results and Discussion

The pump photon energy dependences of the THz waveforms emitted from the GaAs and InP wafers under a fixed bias field of 6.7 kV/cm are shown in Fig. 2. It can be seen that the amplitude and shape of the emitted THz field depend significantly on the pump photon energy both in GaAs and InP. The oscillations observed in the tail of the waveforms at positive excess energies are attributed to the free induction decay of water vapor in the air,[12)] which has a resonance of around 1.6 THz, and is neglected in the following discussion. The absence of such oscillations in the waveforms at negative excess energies is understood by considering the fact that the THz field observed at negative excess energies does not have a significant Fourier amplitude at this frequency because of its long pulse duration.

The observed tendency of the pump photon energy dependence is summarized in Fig. 3, where the peak electric

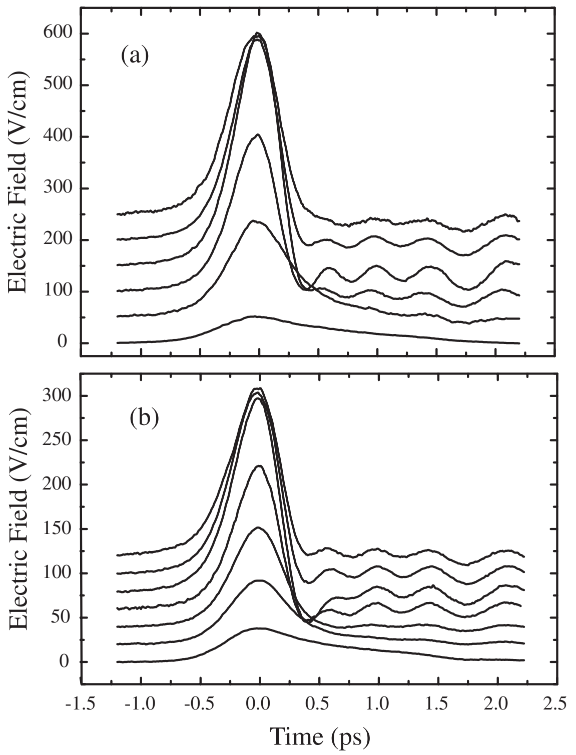

Fig. 2. Temporal waveforms of the THz pulses emitted from (a) GaAs and (b) InP for several excess pump photon energies with respect to band-gap energy. The bias electric field applied to the emitter material was maintained at 6.7 kV/cm. In (a), waveforms are shown for excess energies of −35, −19, −3, 14, 66, and 122 meV from the bottom to the top. Each plot is shifted upward by 50 kV/cm. In (b), waveforms are shown for excess energies of −46, −32, −18, −3, 11, 108, and 198 meV from the bottom to the top. Each plot is shifted upward by 20 kV/cm.

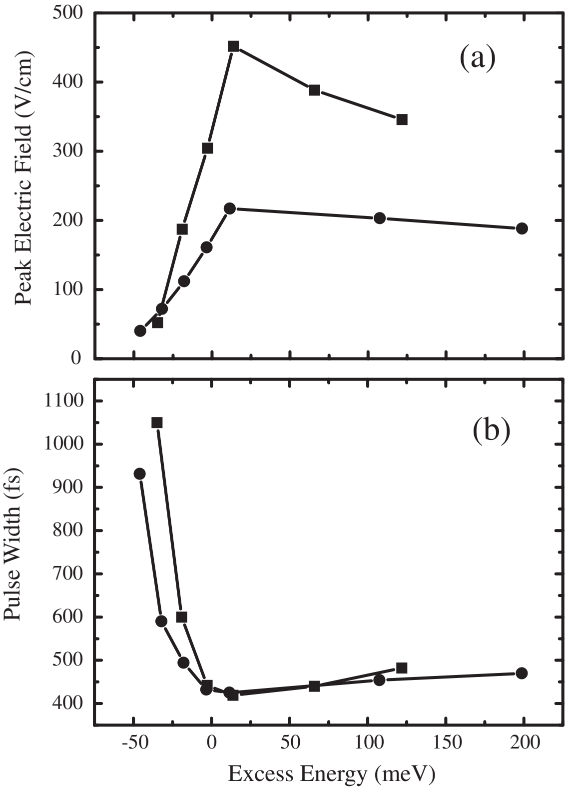

Fig. 3. Peak electric field and temporal width of the emitted THz pulses are plotted as functions of excess energy in (a) and (b), respectively, for GaAs (square) and InP (circle).

field magnitude and the pulse width of the THz pulse are plotted as functions of excess energy. While keeping in mind that the pump pulse has a spectral width of 10 nm, which roughly corresponds to the photon energy of 15 meV, it is seen that the largest field and shortest pulse width are obtained in both GaAs and InP when the entire spectrum of the pump light barely exceeds the band-gap energy. The excess energy dependences of the peak field and the pulse width show a marked change when the sign of the excess energy is changed.

For positive excess energies, the peak field is slightly decreased and the pulse width is slightly increased for large excess energies. The observed THz waveform can be regarded as the time derivative of the time dependence of the transient current induced by the photogeneration of electrons in the emitter materials, as shown in eq. (1). Any contribution of photogenerated holes to the current can be neglected since the mobility of holes is much lower than that of electrons. The electrons having large excess energies have a lower mobility than those at the bottom of the conduction band, due to a larger scattering rate, and relax to the bottom of the band on a sub-picosecond time scale.[2] Correspondingly, the electron mobility is expected to increase on the same time scale,[42] resulting in a slow rise of the current, or a broad THz pulse width. In contrast, when generated using pump light having a photon energy slightly larger than the band-gap energy, electrons are created directly at the bottom of the conduction band, leading to an almost pulse-width-limited rise time of the mobility. Thus, we obtained the shortest and highest THz field at this pump photon energy. Large-aperture photoconductive antennas are widely used for the generation of high-peak-power THz waves, and are most often pumped using 800 nm light obtained from Ti:sapphire laser systems. The present result, however, shows that the most effective THz wave generation is achieved using pump light at 860 nm for GaAs and 910 nm for InP.

At negative excess energies, on the other hand, we observed an exponentially decaying tail in the THz waveforms with a time constant of 1–2 ps, which corresponds to a slow rise in the mobility of electrons generated by photons in this energy region. This energy region corresponds to the Urbach tail.[37–40] The present experimental results show that the electrons excited in the Urbach tail region (Urbach electrons) do not contribute to the macroscopic current immediately after the excitation, and that a transition to a mobile state occurs in 1–2 ps. We believe that the present results are the first experimental observation of the ultrafast dynamics of Urbach electrons. More detailed discussion on Urbach electron dynamics will be given later.

In Fig. 4, we plot the bias field dependence of the peak value of the THz field observed from GaAs and InP at representative excess energies. All the data exhibit a linear dependence of the THz peak field on bias field. This shows that the magnitude of the photoinduced current density, $J(t)$ in eq. (1), depends linearly on the applied bias field. Further examination, however, has clarified that the THz pulse shape depends on the bias field, which shows that the dynamics of current density depends on the bias field.

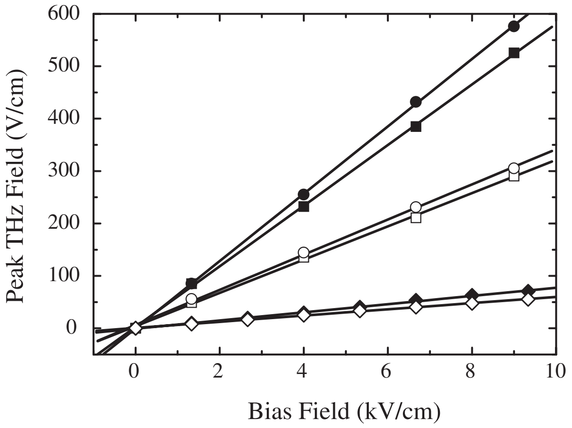

Fig. 4. Bias-field dependences of the peak value of THz field. Symbols show the experimental values; ■, ●, and ◆ are for GaAs at excess energies of 122, 14, and -35 meV, respectively, and □, ○, and ◇ for InP at excess energies of 198, 11, and -46 meV, respectively. Straight lines are the linear fit to the experimental values at each excess energy.

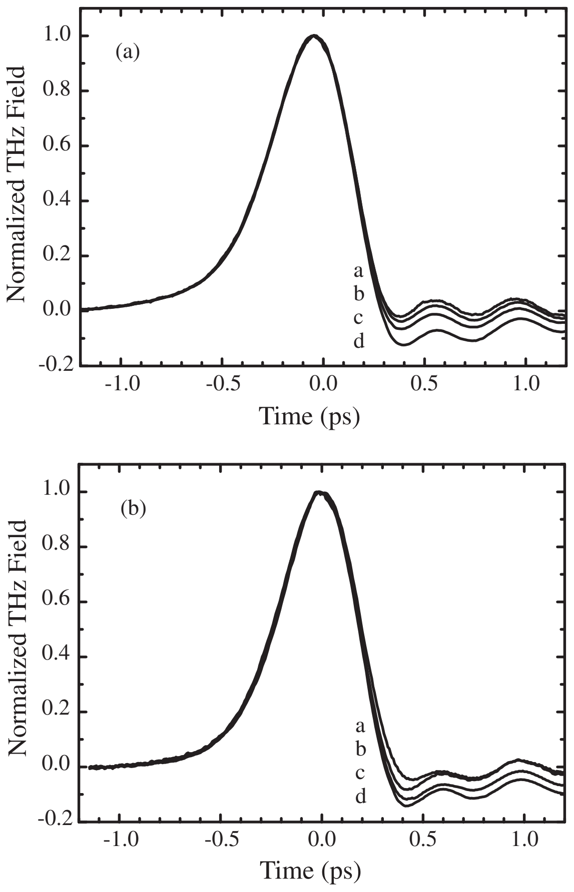

Fig. 5. Bias-field dependences of normalized THz waveforms from GaAs pumped at positive excess energies. (a) Data for excess energy of 122 meV. Lines a, b, c, and d are the waveforms obtained at bias fields of 1.3, 4.0, 6.7, and 9.0 kV/cm, respectively. (b) Data for excess energy of 14 meV. Lines a, b, c, and d are the waveforms obtained at bias fields of 1.3, 4.0, 6.7, and 9.0 kV/cm, respectively.

Figure 5 shows the bias field dependence of normalized THz field waveforms obtained from GaAs at excess energies of 122 and 14 meV. The figure shows that THz waveforms at times longer than 0.4 ps have a small bias field dependence. The THz field in this time region is almost zero, except for oscillations due to water vapor absorption, at a bias field of 1.3 kV/cm, and is negative at 4.0–9.0 kV/cm. The magnitude increases with bias field. This observation shows that the photoinduced current density decreases temporally in this time region at bias fields of 4.0–9.0 kV/cm, while it does not at 1.3 kV/cm. The overshoot effect of transient electron velocity in GaAs at a high electric field has been well studied.[5,6)] Simulation studies[5,6,21)] have shown that the transient electron velocity increases monotonically with time at low bias fields, while it peaks once and subsequently decreases at bias fields greater than 5 kV/cm. The overshoot effect has already been observed in experiments using THz radiation,[17–21)] although these studies focused on current dynamics at bias fields much larger than those of the present study. The present results provide clear experimental evidence showing that the threshold of the overshoot effect lies around a bias field of 4 kV/cm.

Now we will describe the results obtained at negative excess energies, which clarified the dynamics of electrons created in the Urbach tail spectral region. Studies on the spectral shape of the Urbach tail of GaAs have been reported by several groups.[37–40)] Greeff and Glyde[37)] showed from theoretical calculations that the characteristic energy, E_0, of GaAs due to the electron-phonon interaction is about 3 meV at room temperature, and suggested that experimentally observed values,[38–40)] which are larger than this, contains significant contribution from static structural disorder. From our measurements of the transmission spectrum of the GaAs wafer, it was verified that the absorption coefficient of the sample follows the Urbach rule, as shown in eq. (2), below the absorption edge, and we obtained $E_0 = 5.5$ meV, which agrees closely with the reported value of 5.9 meV.[40)] The results of the absorption measurements of the InP sample were consistent with the reported value of $E_0 = 7.1$ meV.[40)] These results suggest that both phonons and crystal disorders play important roles in forming the Urbach tail in our sample materials. Thus, it is expected that both of them also affect the dynamics of Urbach electrons.

The bias field dependence of the temporal waveforms obtained from GaAs at an excess energy of -35 meV is shown in Fig. 6. In Fig. 7, the results obtained from InP at an excess energy of -46 meV are shown. In both figures, the bias field employed was from 1.3 to 9.3 kV/cm. Carrier densities in these measurements were as low as 10^{15} cm^{-3} or less, and conventional spectroscopic techniques such as pump–probe measurements cannot be carried out at this excitation level with an acceptable signal-to-noise ratio. It was observed with both GaAs and InP that the decay of the tail becomes more rapid at larger bias fields. The bias field dependences of the THz waveforms shown in these figures are markedly large than those observed at positive excess energies, as shown in Fig. 5. This shows that the dynamics of Urbach electrons are markedly influenced by relatively small bias fields less than 10 kV/cm. The tails of the THz waveforms were fitted to an exponential function, and the fitted curves are shown as thin lines in Figs. 6 and 7. The obtained decay time constants are plotted as functions of bias field in Fig. 8. The obtained results can be explained by assuming that the electrons created in the Urbach tail region do not contribute to the macroscopic current immediately after being photogenerated and are thermally excited to the

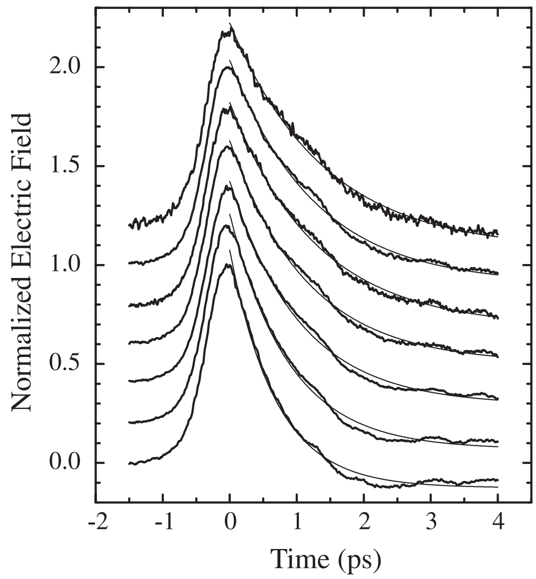

Fig. 6. Thick lines show the bias field dependences of the temporal waveforms of the THz pulses emitted from GaAs pumped at an excess energy of −35 meV. The values of the bias field are 9.3, 8.0, 6.7, 5.3, 4.0, 2.7, and 1.3 kV/cm from the bottom to the top. The time dependence of the electric field at each bias field is normalized and shifted upward by 0.2. Thin lines show the fit of the decaying part to an exponential function.

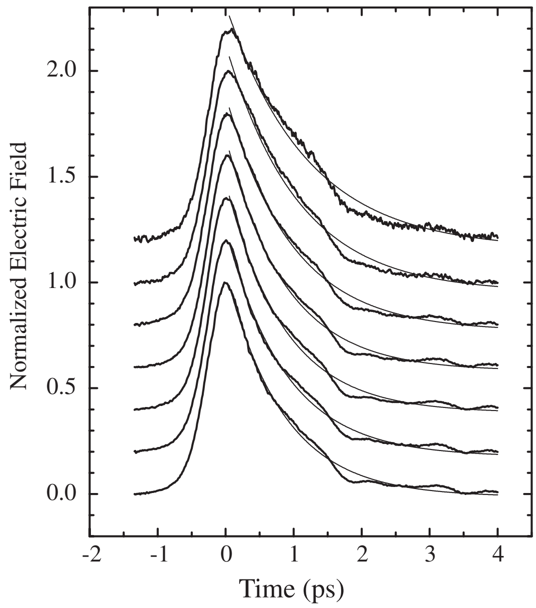

Fig. 7. Thick lines show the bias field dependences of the temporal waveforms of the THz pulses emitted from InP pumped at an excess energy of −46 meV. The bias fields are 9.3, 8.0, 6.7, 5.3, 4.0, 2.7, and 1.3 kV/cm from the bottom to the top. The time dependence of the electric field at each bias field is normalized and shifted upward by 0.2. Thin lines show the fit of the decaying part to an exponential function.

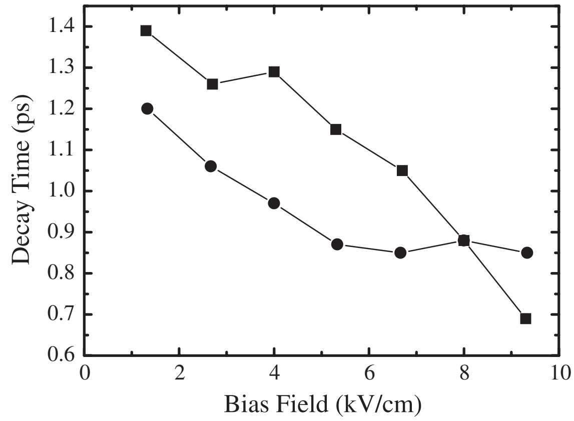

Fig. 8. Bias field dependences of the decay time constant of the exponential fitted curves to the THz field waveforms obtained with pumping photon energy in the Urbach tail region, as shown in Figs. 6 and 7. Black squares correspond to values obtained from GaAs at excess energy of −35 meV and black circles coprrespond to the values obtained from InP at −46 meV.

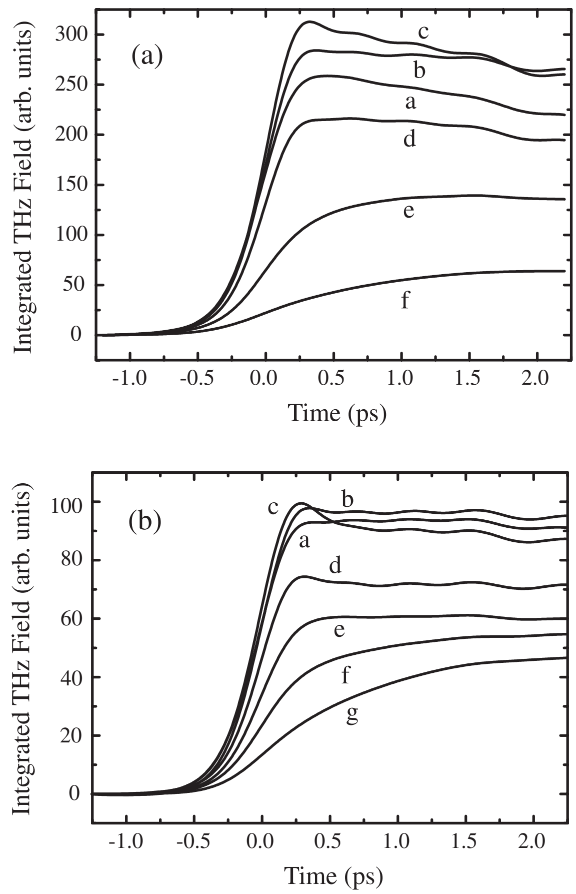

Fig. 9. Time-integrated THz field. Panel (a) shows data for GaAs at excess energies of a: 122 meV, b: 66 meV, c: 14 meV, d: −3 meV, e: −19 meV, and f: −35 meV. Panel (b) shows data for InP at excess energies of a: 198 meV, b: 108 meV, c: 11 meV, d: −3 meV, e: −18 meV, f: −32 meV, and g: −46 meV.

free mobile state with the observed time constant. Dow and Redfield[33)] explained the Urbach tail formation based on the electric-field ionization of excitons in a random potential formed by electron-LO-phonon interaction. They estimated the magnitude of the average effective field of the random potential at 6.9 kV/cm in GaAs, which lies in the observation range of the present study. The fact that a strong field dependence of the THz decay time is observed in this field region shows that the observed current dynamics correspond to the transition of Urbach electrons that are dressed with phonons in the random potential to the free carrier state.

We plot the time-integrated THz field in Fig. 9. From eq. (1), the plotted quantity is regarded as the time-dependent current density induced in the samples. These plots show again that the current rises faster at positive excess energies, and that the rise becomes slower at larger magnitudes of negative excess energies. The time-integrated THz field at 2 ps, where its time dependence becomes almost flat, can be regarded as proportional to the quantum yield of free carriers generated by the photon absorption. Since the yield should be almost unity at positive excess energies, the yields at excess energies of -35 meV for GaAs and -46 meV for InP are estimated to be about 25% and 50%, respectively. When only electron-phonon interaction is assumed, the quantum yield of free carriers from Urbach electrons should be unity.[31–33] We attribute the observed small quantum yields of free carriers at negative excess energies to the fast trapping of Urbach electrons by deep impurity levels, since semi-insulating semiconductors generally have a high density, typically 10^{16}–10^{17} cm^{-3}, of deep trapping sites. Thus, the present results show that imperfections in the crystal, such as defects and impurities, influence the dynamics of Urbach electrons in two different ways: in the formation of the spectral shape of the Urbach tail and in the trapping process after photogeneration.

4. Conclusion

We have studied the ultrafast dynamics of electrons photogenerated at positive and negative excess energies in GaAs and InP by observing the waveform of emitted THz radiation. Sub-picosecond intraband relaxation was observed at positive excess energies. At a high bias field, the overshoot of the transient electron velocity was verified. At negative excess energies, the observed THz waveforms had a tail that decayed in 1–2 ps, which was attibuted to the transition of electrons from the Urbach state to the free carrier state. This dynamical behavior was found to be very sensitive to the field magnitude in the range of several kV/cm. The most effective THz wave generation was achieved using pump light at 860 nm for GaAs and 910 nm for InP.

Acknowledgements

This study was partly supported by KAKENHI (13450026) from the Japan Society for the Promotion of Science.

1) J. Shah: *Ultrafast Spectroscopy of Semiconductors and Semiconductor Nanostructures* (Springer, Berlin, 1999) 2nd ed.
2) A. Othonos: J. Appl. Phys. **83** (1998) 1789.
3) M. C. Nuss, D. H. Auston and F. Capasso: Phys. Rev. Lett. **58** (1987) 2355.
4) E. D. Grann, K. T. Tsen and D. K. Ferry: Phys. Rev. B **53** (1996) 9847.
5) J. G. Ruch: IEEE Trans. Electron Devices **19** (1972) 652.
6) G. M. Wysin, D. L. Smith and A. Redondo: Phys. Rev. B **38** (1988) 12514.
7) D. H. Auston: Appl. Phys. Lett. **43** (1983) 713.
8) C. Fattinger and D. Grischkowsky: Appl. Phys. Lett. **53** (1988) 1480.
9) X.-C. Zhang, B. B. Hu, J. T. Darrow and D. H. Auston: Appl. Phys. Lett. **56** (1990) 1011.
10) J. T. Darrow, X.-C. Zhang, D. H. Auston and J. D. Morse: IEEE J. Quantum Electron. **28** (1992) 1607.
11) E. Budiarto, J. Margolies, S. Jeong, J. Son and J. Bokor: IEEE J. Quantum Electron. **32** (1996) 1839.
12) T. Hattori, K. Tukamoto and H. Nakatsuka: Jpn. J. Appl. Phys. **40** (2001) 4907.
13) T. Hattori, R. Rungsawang, K. Ohta and K. Tukamoto: Jpn. J. Appl. Phys. **41** (2002) 5198.
14) R. Rungsawang, K. Ohta, K. Tukamoto and T. Hattori: J. Phys. D **36** (2003) 229.
15) K. Tukamoto, R. Rungsawang and T. Hattori: Jpn. J. Appl. Phys. **42** (2003) 1609.
16) T. Hattori, K. Ohta, R. Rungsawang and K. Tukamoto: J. Phys. D **37** (2004) 770.
17) J. Son, W. Sha, J. Kim, T. B. Norris, J. F. Whitaker and G. A. Mourou: Appl. Phys. Lett. **63** (1993) 923.
18) J.-H. Son, T. B. Norris and J. F. Whitaker: J. Opt. Soc. Am. B **11** (1994) 2519.
19) A. Leitenstorfer, S. Hunsche, J. Shah, M. C. Nuss and W. H. Knox: Phys. Rev. Lett. **82** (1999) 5140.
20) A. Leitenstorfer, S. Hunsche, J. Shah, M. C. Nuss and W. H. Knox: Phys. Rev. B **61** (2000) 16642.
21) M. Abe, S. Madhavi, Y. Shimada, Y. Otsuka, K. Hirakawa and K. Tomizawa: Appl. Phys. Lett. **81** (2002) 679.
22) Y. Shimada, K. Hirakawa and S.-W. Lee: Appl. Phys. Lett. **81** (2002) 1642.
23) D. You, R. R. Jones, P. H. Bucksbaum and D. R. Dykaar: Opt. Lett. **18** (1993) 290.
24) R. R. Jones, D. You and P. H. Bucksbaum: Phys. Rev. Lett. **70** (1993) 1236.
25) D. J. Cook, J. X. Chen, E. A. Morlino and R. M. Hochstrasser: Chem. Phys. Lett. **309** (1999) 221.
26) M. Usami, T. Iwamoto, R. Fukasawa, M. Tani, M. Watanabe and K. Sakai: Phys. Med. Biol. **47** (2002) 3749.
27) G. Rodriguez and A. J. Taylor: Opt. Lett. **21** (1996) 1046.
28) A. J. Taylor, G. Rodriguez and D. Some: Opt. Lett. **22** (1997) 715.
29) Z. Piao, M. Tani and K. Sakai: Jpn. J. Appl. Phys. **39** (2000) 96.
30) F. Urbach: Phys. Rev. **92** (1953) 1324.
31) H. Sumi and Y. Toyozawa: J. Phys. Soc. Jpn. **31** (1971) 342.
32) H. Sumi and A. Sumi: J. Phys. Soc. Jpn. **56** (1987) 2211.
33) J. D. Dow and D. Redfield: Phys. Rev. B **5** (1972) 594.
34) S. Schmitt-Rink, H. Haug and E. Mohler: Phys. Rev. B **24** (1981) 6043.
35) D. B. Tran Thoai and H. Haug: Phys. Rev. B **47** (1993) 3574.
36) C. H. Grein and S. John: Phys. Rev. B **39** (1989) 1140.
37) C. W. Greeff and H. R. Glyde: Phys. Rev. B **51** (1995) 1778.
38) G. Antonioli, D. Bianchi and P. Franzosi: Phys. Status Solidi B **106** (1981) 79.
39) S. R. Johnson and T. Tiedje: J. Appl. Phys. **78** (1995) 5609.
40) M. Beaudoin, A. J. G. DeVries, S. R. Johnson, H. Laman and T. Tiedje: Appl. Phys. Lett. **70** (1997) 3540.
41) A. Nahata. A. S. Weling and T. F. Heinz: Appl. Phys. Lett. **69** (1996) 2321.
42) A. Gürtler, C. Winnewisser, H. Helm and P. U. Jepsen: J. Opt. Soc. Am. A **17** (2000) 74.